

# TIME AND FREQUENCY DOMAIN IDENTIFICATION AND ANALYSIS OF A PERMANENT MAGNET SYNCHRONOUS SERVO MOTOR

Jui-Jung Liu, Ya-Wei Lee, Fu-Cheng Wang, Ramesh Uppala, and Ping-Hei Chen\*

## ABSTRACT

This study employed the approach of non-linear autoregressive moving average model with exogenous inputs (NARMAX) to analyze the dynamics of a Permanent Magnet Synchronous Motor (PMSM). The non-linearity in PMSM including cogging force, reluctance force and force ripple is difficult to estimate. By using the NARMAX approach, thrust-speed relationship and thrust-position relationship could be analyzed by identifying both time and frequency domain models of the system. The frequency domain analysis is studied by mapping the discrete-time NARMAX models into generalized frequency response functions (GFRFs) to reveal the non-linear coupling between the various input spectral components and the energy transfer mechanisms in the system. From the results, the interpretation of the higher-order GFRFs has been comprehensively studied and non-linear effects have been related to the physical models of the systems.

**Key Words:** Identification; non-linear system, frequency response functions.

## I. INTRODUCTION

Many Permanent magnet synchronous motor (PMSM) response studies have been carried out using various approaches for modelling the speed and torque control system (Jahns and Soong, 1996; Solsona *et al.*, 2000; Bolognani *et al.*, 2001). These investigations may be classified into time domain and frequency domain methods, which involve numerical integration of motions, neuro fuzzy optimization techniques and experimental estimation. These methods are well suited to explain many of the non-linear dynamic behaviours associated with PMSM systems. Cheng and Tzou (2004) developed a novel design approach by applying gradient optimization with step-sizing techniques to design a digital PMSM servo drive, and the servo responses were then fed back to evaluate the overall system performances. Hattori *et*

*al.* (2001) projected a suppression control method which used repetitive control with auto-tuning function and Fourier transform to the motor frame vibration and the rotational speed vibration. Yue *et al.* (2003) derived a mathematical model of PMSM with initial rotor position uncertainty and proposed the control methodology. Babak *et al.* (2004) provided an online identification method to limit the parameter uncertainties. This method did not need a well-known initial rotor position and made the sensorless control more robust with respect to the stator resistance variations at low speed. All these studies have been extensively explored, studied and documented by (Driss *et al.*, 2001; Mobarakeh *et al.*, 2001; Morimoto *et al.*, 2002). Frequency domain methods are quite efficient for performing stochastic analysis. However, prior to frequency domain analysis a Fast Fourier Transform (FFT) is usually employed to transform the time domain signal to a spectrum distribution on a linear frequency domain (Kadjoudj *et al.*, 2001; 2003; 2004). Therefore, the dynamic characteristics of a nonlinear system could be shown by the power spectral density (PSD) derived from experimental data.

Actually, cross modulation, desensitization, and

\*Corresponding author. (Tel: 886-2-33662689; Fax: 886-2-23670781; Email: phchen@ntu.edu.tw)

J. J. Liu is with the Department of Information and Electronic Commerce, Kainan University, Taoyuan 338, Taiwan

Y. W. Lee, F. C. Wang, R. Uppala, and P. H. Chen are with the Department of Mechanical Engineering, National Taiwan University, Taipei 106, Taiwan

gain compression/expansion may exist simultaneously, which are generated within frequencies, and these cause nonlinear phenomena in the frequency domain. Analysis of non-linear systems in the frequency domain is advantageous as integral equations which relate the input-output in the time domain become algebraic in the frequency domain. In academia, non-linear system analysis and prediction to a gray or black system have been an important issue, but many studies described non-linear systems just by a linear approach in consideration of the complicated estimation process. The present study is based on the NARMAX (Non-linear Auto-Regressive Moving Average with eXogenous inputs) (Leontaris and Billings, 1985; Billings and Voon, 1986; Billings *et al.*, 1989; Brown and Harris, 1994) modelling technique to build a model which can predict the rotor velocity and position accurately. Thereafter, by applying a recursive probing algorithm to NARMAX models, it is possible to obtain the non-linear frequency response functions of real systems so that the analysis and application of non-linear transfer functions become more practical.

Recently, system identification has become a very active subject in research. Thouverez and Jezequel (1996) used the modal co-ordinates to express the NARMAX model which reduced the number of parameters to identify a mass-spring system. Liu *et al.* (2001) proposed a new graphical user interface interpretation tool for the non-linear frequency response function, and demonstrated the improved visualization of the multi-dimensional non-linear generalized frequency responding functions (GFRFs). The present study is based on a combined approach of both the time and the frequency domains. It is shown that new insights into PMSM dynamics can be obtained from studying both time and frequency domain properties of the system. The non-linear GFRFs, which are generalizations of the linear frequency response functions, are shown to be crucial in system interpretation and modelling.

The thrust-speed and magnetic thrust-position relationships of PMSM are extensively studied in this paper. After a presentation of the NARMAX approach and frequency domain concepts, the identification and analysis results of PMSM model are presented in both time and frequency domain.

## II. TIME AND FREQUENCY DOMAIN IDENTIFICATION TECHNIQUES

### 1. The NARMAX Approach

A wide class of discrete time multi-variable non-linear stochastic systems, can under appropriate assumptions, be represented by the NARMAX model. For an  $m$ -output  $r$ -input system, it can be described as follows:

$$\begin{aligned} \underline{y}(k) = & \underline{\alpha} + \underline{F}^{\ell}[\underline{y}(k-1), \dots, \underline{y}(k-n_y), \underline{u}(k-d), \\ & \dots, \underline{u}(k-d-n_u), \\ & \underline{\varepsilon}(k-1), \dots, \underline{\varepsilon}(k-n_{\varepsilon})] + \underline{\varepsilon}(k) \end{aligned} \quad (1)$$

where

$$\underline{y}(k) = \begin{bmatrix} y_1(k) \\ \vdots \\ y_m(k) \end{bmatrix}, \quad \underline{u}(k) = \begin{bmatrix} u_1(k) \\ \vdots \\ u_r(k) \end{bmatrix}, \quad \underline{\varepsilon}(k) = \begin{bmatrix} \varepsilon_1(k) \\ \vdots \\ \varepsilon_m(k) \end{bmatrix}$$

in which  $\underline{y}(k)$ ,  $\underline{u}(k)$  and  $\underline{\varepsilon}(k)$  represent the system output, input and prediction error respectively.  $d$  is the system time delay.  $\ell$  is the degree of non-linearity and  $\underline{\alpha}$  is a constant vector term to accommodate mean levels.  $\underline{F}[\cdot]$  is a vector valued non-linear function. Taking the  $i^{\text{th}}$  row from Eq. (1) with different values of the maximum lag for each output, input and noise gives

$$\begin{aligned} y_i(k) = & \alpha + F_i^{\ell}[y_1(k-1), \dots, y_1(k-n_{y1}^i), \dots, \\ & y_m(k-1), \dots, y_m(k-n_{ym}^i), \\ & u_1(k-d), \dots, u_1(k-d-n_{u1}^i), \dots, u_r(k-d), \dots, \\ & u_r(k-d-n_{ur}^i), \\ & \varepsilon_1(k-1), \dots, \varepsilon_1(k-n_{\varepsilon}), \dots, \varepsilon_1(k-n_{\varepsilon}^i), \dots, \varepsilon_m(k-1), \\ & \dots, \varepsilon_m(k-n_{\varepsilon m}^i)] + \varepsilon_i(k), \quad k = 1, \dots, m \end{aligned} \quad (2)$$

When  $m = r = 1$ , the model of Eq. (2) reduces to the single-input single-output (SISO) case as follows:

$$\begin{aligned} y(k) = & \alpha + F^{\ell}[y(k-1), \dots, y(k-n_y), u(k-d), \dots, \\ & u(k-d-n_u), \varepsilon(k-1), \dots, \varepsilon(k-n_{\varepsilon})] + \varepsilon(k) \end{aligned} \quad (3)$$

where  $\varepsilon(k)$  is the residue at time  $k$ .

Tsang and Billings (1994) used an orthogonal estimator for the identification of NARMAX models. The orthogonal estimator is a simple and efficient algorithm that allows each coefficient in the model to be estimated. At the same time, it provides an indication of the contribution that each term makes to the system output, using the error reduction ratio (ERR). In this study, when eliminating the dc offset, ERR can be defined as

$$ERR_i = \frac{\sum_{k=1}^N g_i^2 w_i^2(k)}{\sum_{k=1}^N y^2(k) - \frac{1}{N} [\sum_{k=1}^N y(k)]^2} \times 100\% \quad (4)$$

where  $g_i$  are the coefficients and  $w_i$  are the terms of an auxiliary model constructed in such a way that the terms  $w_i$  are orthogonal to the data records. A forward-regression algorithm is employed at each step to select the term with the highest ERR, in other words, the term that contributes most to the reduction of the residual variance.

The ERR value can be computed together with the parameter estimation to indicate the significance of each term, then the terms can be ranked according to their contribution to the overall mean squared prediction error.

## 2. Non-linear Systems Higher-order Frequency Response Functions Analysis and Interpretation

The discrete polynomial NARMAX representation of a particular system is not necessarily unique. If the model captures the system dynamics correctly, no matter in what form the discrete model is, it must present the correct linear and non-linear frequency content of the system. In other words, even though there may be a number of discrete time models to represent a real system, the higher-order GFRFs corresponding to each of the discrete models should be unique.

Most conventional non-linear frequency domain representations have been based on the extensions of FFT routines to the Volterra model. A better approach, based on the estimation of parameters of a NARMAX model, has been proposed by Lang and Billings (2000), which is then used to generate the GFRFs. The advantage of using the polynomial NARMAX model is the reduction of the number of parameters which encode information from past outputs and past inputs, and the smaller data set required for identification. The NARX model can be obtained from the NARMAX model by eliminating the error terms.

$$y_m(k) = \sum_{p=0}^m \sum_{\ell_1, \ell_{p+q}=1}^L c_{p,q}(\ell_1, \dots, \ell_{p+q}) \prod_{i=1}^p y(k-\ell_i) \cdot \prod_{j=p+1}^{p+q} u(k-\ell_j) \quad (5)$$

$$y(k) = \sum_{m=1}^M y_m(k) \quad (6)$$

where  $y_m(k)$  indicates the  $m^{\text{th}}$  order output signal, and  $c_{p,q}(\ell_1, \dots, \ell_{p+q})$  donates the coefficient of product of  $\prod_{i=1}^p y(k-\ell_i)$  and  $\prod_{j=p+1}^{p+q} u(k-\ell_j)$ .

Transferring Eq. (6) to frequency domain, the frequency responding function can be found as (Thouverez and Jezequel, 1996):

$$\begin{aligned} & [1 - \sum_{\ell_1=1}^L c_{1,0}(\ell_1) e^{-j2\pi(f_1 + \dots + f_n)\ell_1}] H_n^{\text{asym}}(f_1, \dots, f_n) \\ &= \sum_{\ell_1, \ell_n=1}^L c_{0,n}(\ell_1, \dots, \ell_n) e^{-j2\pi(f_1\ell_1 + \dots + f_n\ell_n)} \\ &+ \sum_{q=1}^{n-1} \sum_{p=1}^{n-q} \sum_{\ell_1, \ell_N=1}^L c_{p,q}(\ell_1, \dots, \ell_{p+q}) \\ &\cdot e^{-j2\pi(f_{n-q}\ell_{n-q+1} + \dots + f_{p+q}\ell_{p+q})} H_{n-q,p}(f_1, \dots, f_{n-q}) \\ &+ \sum_{p=2}^n \sum_{\ell_1, \ell_2=1}^L c_{p,0}(\ell_1, \dots, \ell_p) H_{n,p}(f_1, \dots, f_n) \quad (7) \end{aligned}$$

where  $H$  is frequency responding function. The regressive relation can be written as

$$H_{n,p}^{\text{asym}}(\cdot) = \sum_{i=1}^{n-p+1} H_i^{\text{asym}}(f_1, \dots, f_i) H_{n-i,p-1}(f_{i+1}, \dots, f_n) e^{-j2\pi(f_1, \dots, f_i)\ell_p} \quad (8)$$

The symmetry of an  $n^{\text{th}}$  order frequency responding function is defined as

$$H_n^{\text{sym}}(f_1, \dots, f_n) = \frac{1}{n!} \sum_{\pi} H_n^{\text{asym}}(f_{\pi(1)}, \dots, f_{\pi(n)}) \quad (9)$$

where  $\pi$  indicates all permutations of  $f_1, \dots, f_n$  in  $H_n(\cdot)$ .

The higher-order frequency responding functions deduced from NARX model can represent multi-dimensional characteristics and be used to investigate the dynamic behavior of a real system.

## 3. Model Validation

A strategy to evaluate the model correctness and validity is indispensable once the significant terms have been identified and estimation of associated parameter values has been obtained. If validation shows that the model is not good, some of the design variables of the estimation should be changed and the identification procedure should be repeated. Three ways of validating a model are used in this study:

1. One-step ahead prediction and model predicted output: the one-step ahead prediction of the output is defined as

$$\begin{aligned} \tilde{y}(k) &= \tilde{F}^\ell[y(k-1), \dots, y(k-n_y), u(k-d), \dots, \\ &u(k-d-n_u), \varepsilon(k-1, \tilde{\theta}), \dots, \varepsilon(k-n_\varepsilon, \tilde{\theta})] \quad (10) \end{aligned}$$

where  $\tilde{F}[\cdot]$  is the estimate of  $F[\cdot]$ ,  $\varepsilon(k, \tilde{\theta})$  is the residue given by

$$\varepsilon(k, \tilde{\theta}) = y(k) - \tilde{y}(k). \quad (11)$$

This is a by-product of the regression process. From Eq. (10) the prediction is easily obtained by subtracting the prediction errors from the original data. At each step the model is effectively reset by inserting the appropriate values into the right hand side of Eq. (10) and any error is therefore reset at each step. Consequently, even a poor model can produce reasonable one-step ahead predictions. For these reasons, the one-step ahead predictions do not often provide a good metric of model performance.

The model predicted output (MPO) is defined as

$$\tilde{y}_{MPO}(k) = \tilde{F}^l[\tilde{y}(k-1), \dots, \tilde{y}(k-n_y), u(k-d), \dots, u(k-d-n_u), 0, \dots, 0] \quad (12)$$

where the measured inputs are used to generate the model output. The zeros are present because the prediction errors will not be available when using the model to predict the output. It is an essential condition for accepting the model that the estimated model predicted outputs are in good agreement with the measured outputs.

2. Cross-validation test: estimated models are usually validated using an independent set of data called the validation data (test set). This is usually referred to as cross-validation. The output from the model and the system are compared when they are run with the same input where the input data has not previously been used in the identification. The difference between the system output and MPO has to be as small as possible. The comparison between the observed data and the model output usually reveals much with regard to model anomalies not previously detected. Failure to pass the cross-validation test may also indicate that the system is not time-invariant.
3. Model validity test (correlation tests): The approach consists of computing the auto-correlation function of the residues and the cross-correlation functions between the residues and the inputs. In order to extend to non-linear models, practical tests must be available to check the presence of non-linearity in both raw time series and residues from the fitted models. Many tests have been proposed, but using higher-order correlation functions for validity of non-linear systems has been successful.

When the system is non-linear the residues should be unpredictable from all linear and non-linear combinations of past inputs and outputs. This will be true if the following correlation tests are satisfied

$$\begin{aligned} \phi_{\varepsilon\varepsilon}(\tau) &= \delta(\tau), \phi_{u\varepsilon}(\tau) = 0 \quad \forall \tau, \phi_{u^2\varepsilon}(\tau) = 0 \quad \forall \tau, \\ \phi_{u^2\varepsilon^2}(\tau) &= 0 \quad \forall \tau, \phi_{\varepsilon u}(\tau) = 0 \quad \forall \tau \geq 0 \end{aligned} \quad (13)$$

where  $\phi_{ab}(\tau) = E[a(k-\tau)b(k)]$ ,  $\delta(\tau)$  is the Kronecker delta,  $u(\tau)$  and  $\varepsilon(\tau)$  are the input and the residues sequence, respectively, and the single quote indicates that the mean has been removed.

### III. ANALYSIS OF THE PMSM

Permanent Magnet Synchronous Motor (PMSM) drives have gained considerable attention among researchers recently because of several advantages. The high torque density, small size, inherent variable speed capability, and overall high performance of the drive with appropriate control strategy are some of the positive aspects of the PMSM drive. Generally, for this kind of motor the individual phase excitations are synchronized with rotor position, which necessitates position sensing. Usually, mechanical position sensors, like resolvers or optical encoders, are employed for this purpose. External position sensors, however, give position information with high resolution and accuracy, but they have certain drawbacks. Position sensors with good accuracy are usually expensive and they need proper mechanical mounting. They occupy space, and the cabling associated with sensors needs to be shielded in order to avoid corruption due to external noise. Several methods have been published in the literature on sensor elimination techniques with which the rotor information is obtained electronically.

Because of high efficiency and linearity between torque and current, the PMSM has been widely used in many industrial applications. The position and speed sensors, which are normally mounted on PMSM, are desirable to eliminate from the standpoints of machine size, weight, cost, and reliability.

#### System Description

There are two applications included in this experimental design. First, under standard interference, non-linear identification methodology is adopted to construct the NARX models by using I/O signals of PMSM. These discrete non-linear models for PMSM contain the lag of inductance and uncertain electrical factors. Secondly, mapping of the NARX models into frequency domain, then multi-dimensional dynamic behavior of systems can be shown by high order GFRFs.

The main framework of the experiment consists of a PMSM set, motor drive interface, power amplifier, Hall sensor and a control PC (Fig. 1). The measuring system is developed by real time control driving interface of a PMSM with visualized modules. When  $e$  control operations are executed, the feedback signals and control commands are transmitted by the interface card, through an ISA Bus, to the control PC. After computations, three-phase output voltage is

**Table 1** Specification of test motor

Parameter	Value	Unit
Rated output	83	W
Rated speed	1.0	m/sec
Rotor equivalent resistor per phase ( $R_s$ )	11.6504/3.0	$\Omega$
Rotor inductance per phase ( $L_s$ )	0.0048/3.0	H
Stator flux ( $\lambda_m$ )	0.4849	Wb
Standard rotor mass (M)	2.3213	kg
Viscous friction coefficient (B)	32.4992	N/m/s

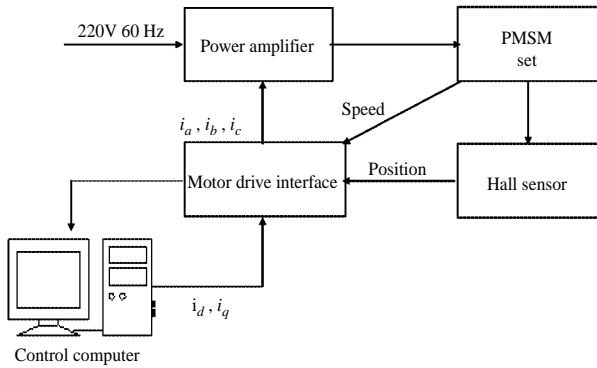


Fig. 1 Experimental system configuration

obtained. A real time control circle of PMSM is completed by transmitting this output voltage to the motor driving interface card by the same ISA Bus. The specifications of the test motor are shown in Table 1.

#### IV. TIME DOMAIN IDENTIFICATION

The PMSM has a permanent magnet (PM) on the rotor and requires alternating stator currents to produce constant torque. Besides, the PMSM has sinusoidal induced electromotive-force (the so-called back-emf) which contributes to the operating characteristics. In this study, electromagnetic thrust is regarded as input; rotor speed and position are regarded as the output. Due to the variance of operating time, environmental effects, or man-made errors, the parameters of PMSM may lead to bias. For this reason, accurate prediction can hardly be achieved. In this study, using a NARMAX approach to build a NARX model which represents a real PMAM system, the error term  $\varepsilon$  would be obtained from subtracting the predicted output  $\tilde{y}$  from the actual output.

##### 1. Thrust-Speed NARX Model

The data are sampled at a rate of 500 Hz. The input data representing the electromagnetic thrust is given as sinusoidal waves which are fed into the

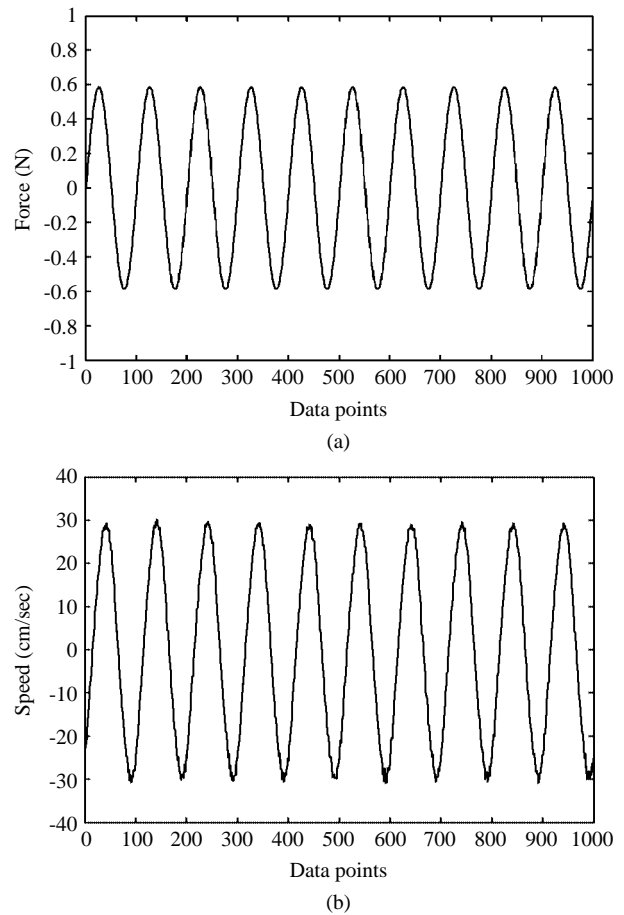


Fig. 2 Input (a: thrust) and output (b: speed) of data set taken from the 1001st to 2000th samples

PMSM, while the output data is the rotor speed. Data points from 1001 to 2000 of I/O data are assumed for estimation set, and data points from 3001 to 4000 of I/O data are assumed for validation set. The I/O time series signals for validation set are shown in Fig. 2.

First, the power spectral density (PSD) plots of input thrust and output speed are illustrated in Fig. 3. It shows that the input and output energy occurred around the normalized frequency 0.033 but the energy magnitude expanded by several orders. This suggests that the system possesses non-linear dynamics around this frequency caused by electrical parameter variations. This non-linear effect would directly relate to model structures, time delays, etc. Structure selecting is important to identify the non-linearity of a system. In this study, a quadratic NARX model is considered and the model structure is designed for 15 terms by rule of thumb. Setting appropriate time lags will help to describe the real system and could avoid computation problems, and the appropriate maximum time lags should be set as 40 and 30 to input and output respectively for this case. It means that predicted output would be simulated by the combinations of 40 input signals and



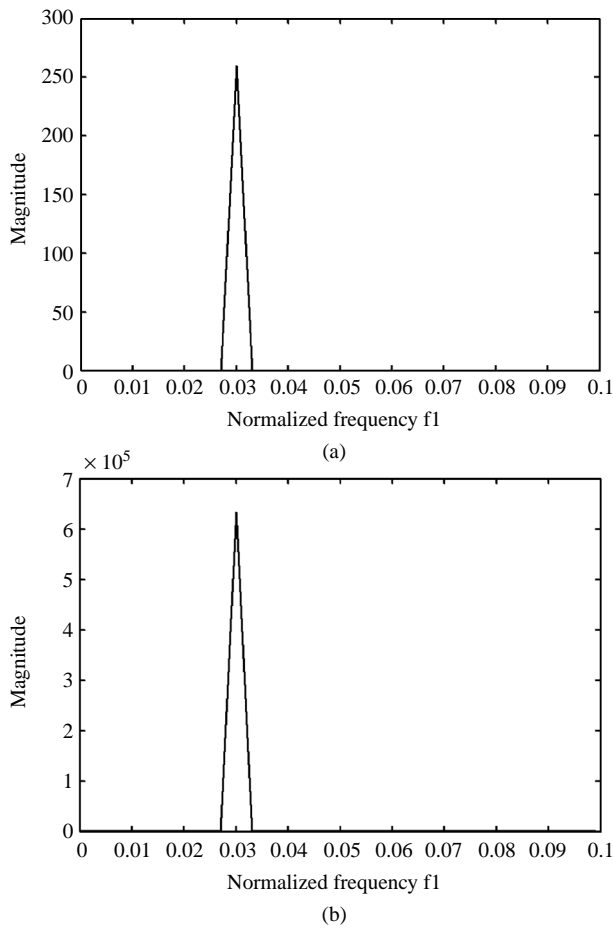


Fig. 3 Power spectral density of (a) input signal (thrust) and (b) output signal (velocity)

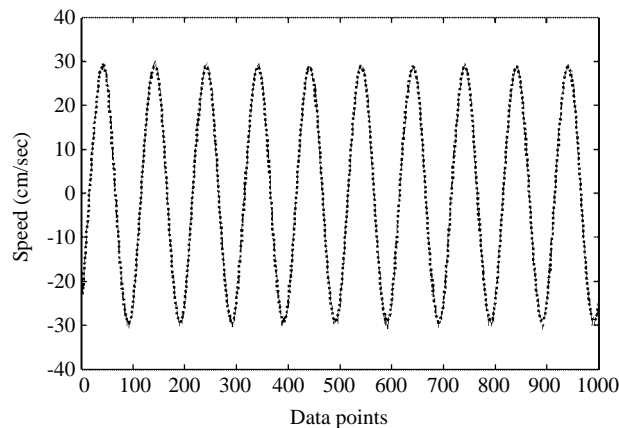


Fig. 4 Comparison of the model predicted output (dotted line) with the original measurements (solid line)

30 output signals. The estimation result of the I/O relationship is represented as a difference equation in Table 2. The model predicted output and cross-validation tests are shown in Figs. 4 and 5 respectively where the model predicted output follows the system

Table 2 Quadratic thrust-speed NARX model

Model parameter	Estimate	ERRi	Standard deviation
$u(k-14)$	0.33710 e+2	0.9976	0.0432
$y(k-1)$	0.31254	0.1083 e-2	0.0308
$y(k-14)$	-0.90502 e-1	0.9426 e-4	0.0264
$y(k-30)$	0.13787	0.6672 e-4	0.0252
$y(k-33)u(k-21)$	0.38805	0.3426 e-4	0.0798
$y(k-23)$	-0.10185	0.3133 e-4	0.0272
$y(k-5)$	0.96491 e-1	0.1948 e-4	0.0304
$y(k-26)$	0.10947	0.1834 e-4	0.0259
$y(k-18)$	-0.90082	0.1563 e-4	0.0268
$y(k-9)$	-0.11602	0.1187 e-4	0.0271
$y(k-6)$	0.86075 e-1	0.1042 e-4	0.0305
$y(k-2)$	0.91110 e-1	0.9358 e-5	0.0305
$y(k-7)y(k-33)$	-0.33757 e-2	0.6161 e-5	0.0012
$y(k-3)y(k-32)$	-0.34004 e-2	0.5636 e-5	0.0009
$y(k-16)y(k-36)$	-0.13394 e-2	0.1190 e-5	0.0004

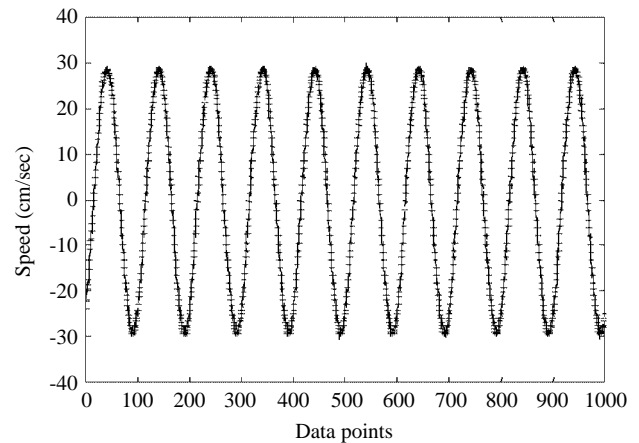


Fig. 5 Cross-validation test: original measurements (solid line) and model (asterisk line)

output very well. It means that this time domain speed model can simulate the output speed completely and it can also play a role in speed prediction. Besides, the system is proved time-invariant. The model validity tests shown in Fig. 6 indicate that the model is reasonable because the model validity tests are all inside the confidence bands except  $\phi_{u^2 \varepsilon^2}(k)$  which is just outside. It shows that this estimated model can grasp the dynamics of the PMSM precisely. This model is validated by cross validation test, correlation tests and model output prediction test, so the estimated non-linear NARX model is quite reliable to identify the relationship between electromagnetic torque and output speed of a PMSM.

## 2. Thrust-Position NARX Model

In this case, a thrust-position model is estimated

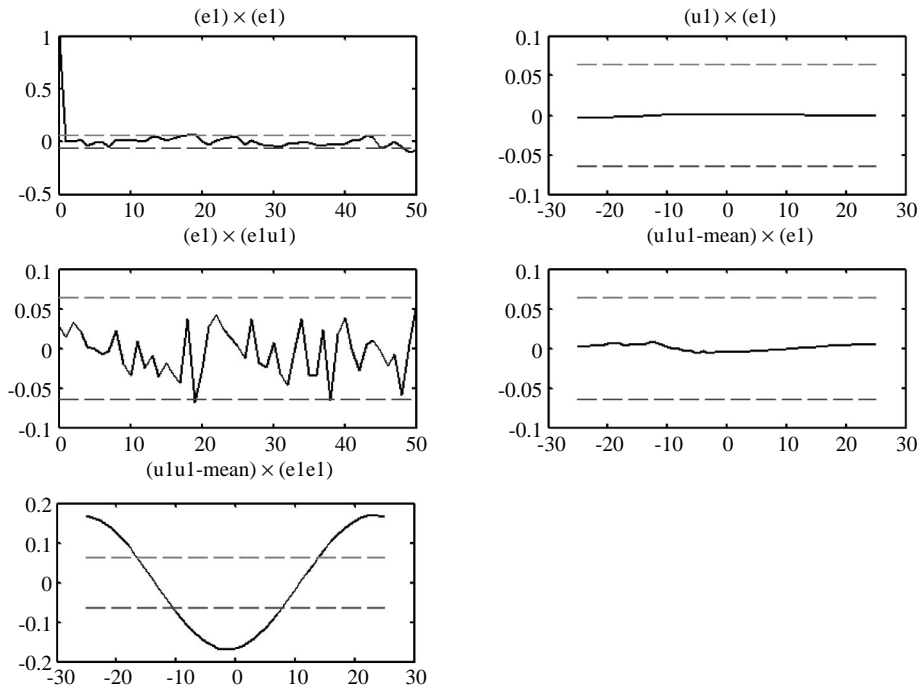


Fig. 6 Model validity tests

by the same method as above. The input is the measured electromagnetic torque as sinusoidal waves and sampled at 500 Hz, and the output is the rotor position varied by the magnetic thrust. Assuming data points from 1001 to 2000 of I/O data are the data set for estimation, and data points from 3001 to 4000 of I/O data are for validation. The I/O time series signals for validation set are shown in Fig. 7.

The PSD of the input thrust and output position are illustrated in Fig. 8. It shows that the input energy is around the normalized frequency 0.023 and the output energy frequency is around the normalized frequency 0.023 and 0. This result indicates that there exists obvious non-linearity in this system. Energy transfer occurs around a specific frequency, and this phenomenon results in several order growth in the PSD magnitude from input to output signals. A quadratic NARX model is built. The maximum time lags are set as 10 to both input and output, and the estimation result of the I/O relationship is represented as a difference equation listed in Table 3. The model predicted output and cross-validation test are shown in Fig. 9 and 10 respectively. The good results mean that this non-linear model can describe the real system completely, and the output position can be predicted by the model. In Fig. 11, all the model validity tests satisfy the 95% confidence limit except  $\phi_{u^*e^*}(k)$  which is just outside. It shows that this estimated model can grasp the dynamics of the system. This model is also validated by the three tests, namely the cross validation test, the

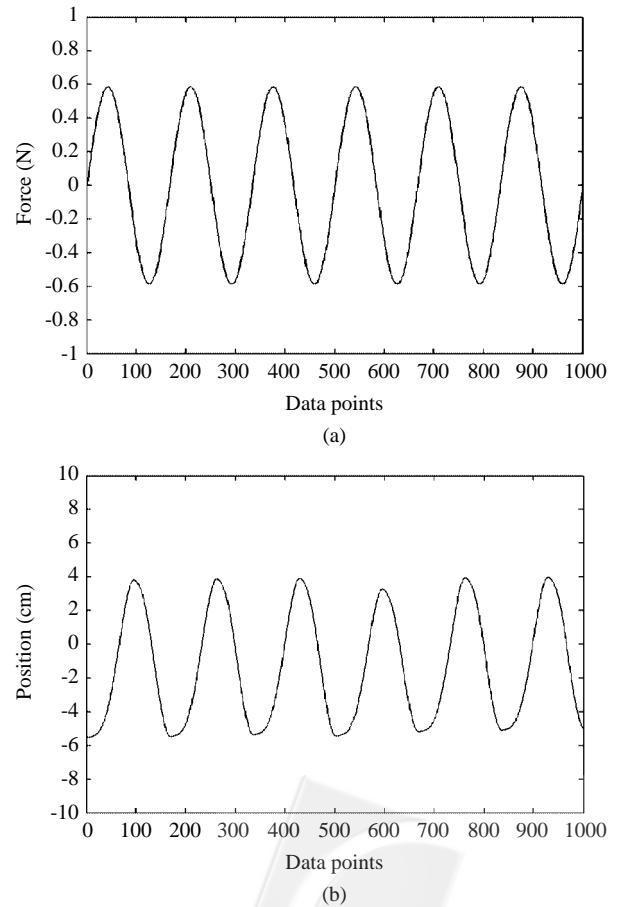


Fig. 7 Input (a: thrust) and output (b: position) of data set taken from the 1001st to 2000th samples

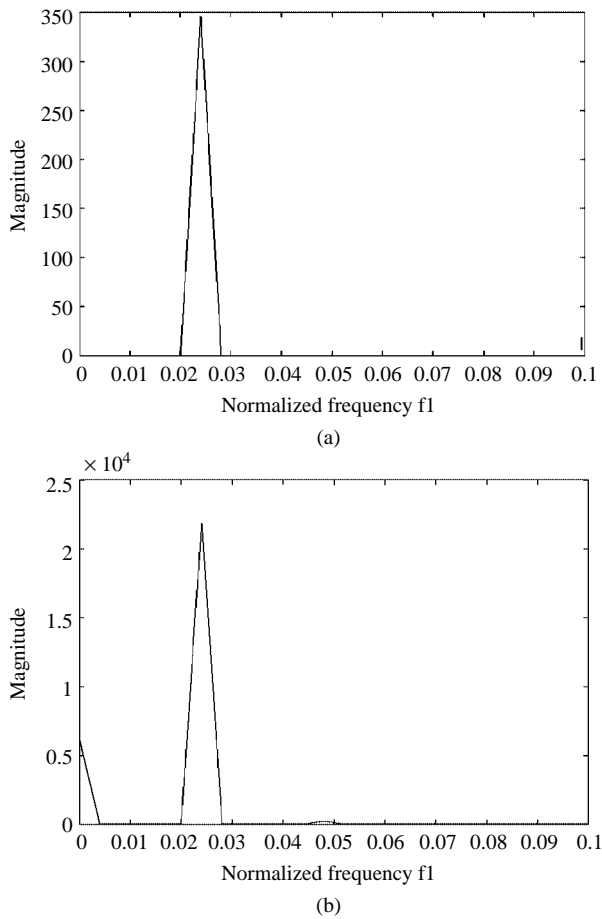


Fig. 8 Power spectral density of (a) input signal (thrust) and (b) output signal (position)

correlation tests and the model output prediction test, so that the non-linear NARX model is a qualified model to identify the relationship between the thrust and position of a PMSM.

## V. FREQUENCY DOMAIN ANALYSIS

The interpretation of non-linear effects in the frequency domain is illustrated by the higher order frequency functions computed using the models in Tables 1 and 2. The GFRFs can be directly derived from NARMAX models according to Eqs. (7) and (8). In speed NARMAX model, the first-order frequency response function  $H_1(f)$  is illustrated in Fig. 12. The resonances in  $H_1(f)$  are found approximately at 0.033 in normalized frequency and the corresponding magnitude is 50 dB. The non-linear GFRFs are generated by the non-linear terms in the discrete-time models. The second-order GFRFs  $H_2(f_1, f_2)$  are derived and represented in Fig. 13. There are four dominant ridges along equations  $f_1 = 0.033$ ,  $f_2 = -0.033$ ,  $f_1 + f_2 = 0.033$  and  $f_1 + f_2 = -0.033$ . Since the sampling

Table 3. Quadratic thrust-position NARX model.

Model parameter	Estimate	ERRi	Standard deviation
$y(k-1)$	0.22209 e+1	0.9986	0.0303
$y(k-2)$	-0.15159 e+1	0.1349 e-2	0.0611
$y(k-9)$	0.60831	0.5348 e-6	0.0612
$u(k-10)$	0.27583 e-1	0.3539 e-7	0.0029
$y(k-8)$	-0.48565	0.5302 e-7	0.0361
$y(k-3)$	0.34624	0.4279 e-7	0.0357
$y(k-10)$	-0.17312	0.3770 e-7	0.0301
$y(k-1)u(k-10)$	0.33725 e-2	0.2140 e-7	0.0027
$y(k-10)y(k-10)$	-0.73095 e-2	0.1082 e-7	0.0030
$y(k-2)u(k-2)$	0.26377 e-3	0.9794 e-8	0.0027
$y(k-1)y(k-1)$	0.12182 e-1	0.1187 e-8	0.0037
$y(k-4)y(k-4)$	0.32931 e-1	0.3206 e-8	0.0049
$y(k-6)y(k-6)$	-0.23274 e-1	0.8147 e-8	0.0039
$y(k-2)y(k-2)$	-0.28863 e-1	0.6589 e-8	0.0063
$y(k-9)y(k-9)$	0.14489 e-1	0.4357 e-8	0.0045

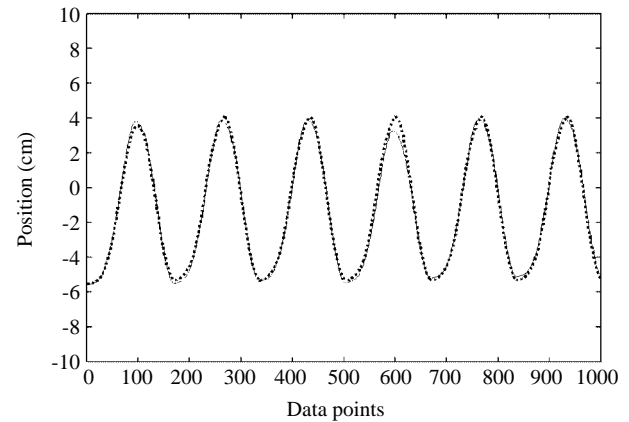


Fig. 9 Comparison of the model predicted output (dotted line) with the original measurements (solid line)

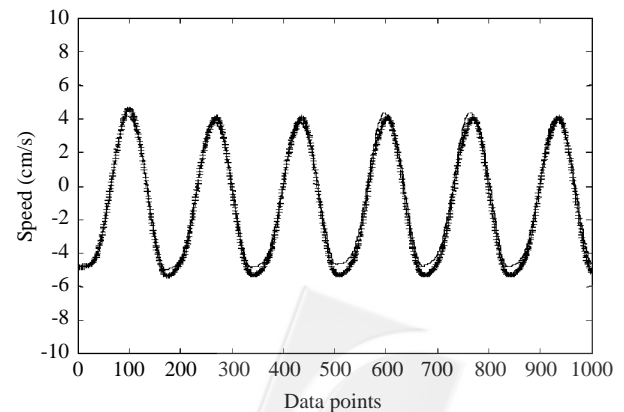


Fig. 10 Cross-validation test (original measurements: solid line; model: asterisk line)



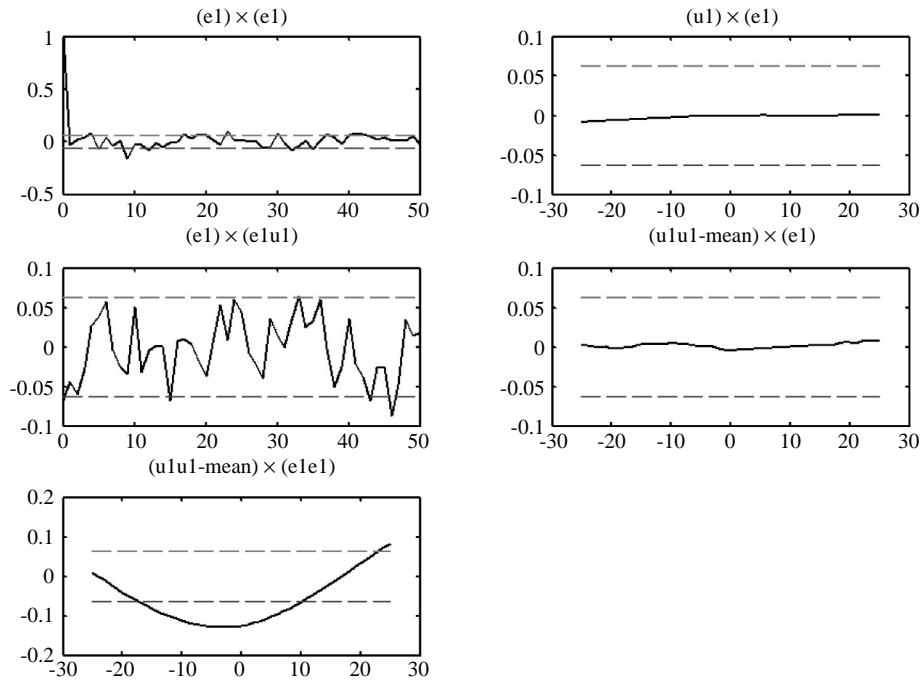


Fig. 11 Model validity tests.

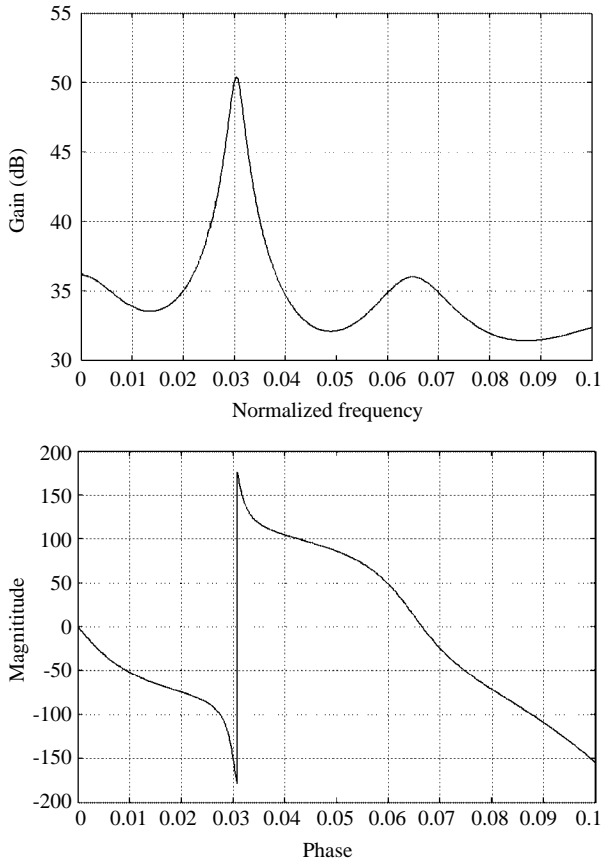


Fig. 12 The first-order GFRFs and phase angle of thrust-speed model

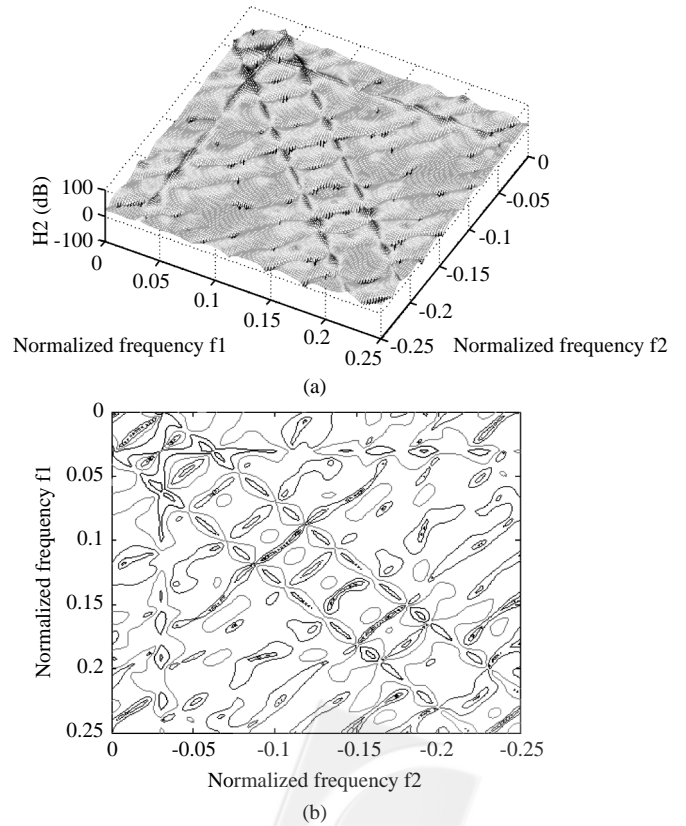


Fig. 13 The second-order GFRFs of thrust-speed model: (a) top view, and (b) contour

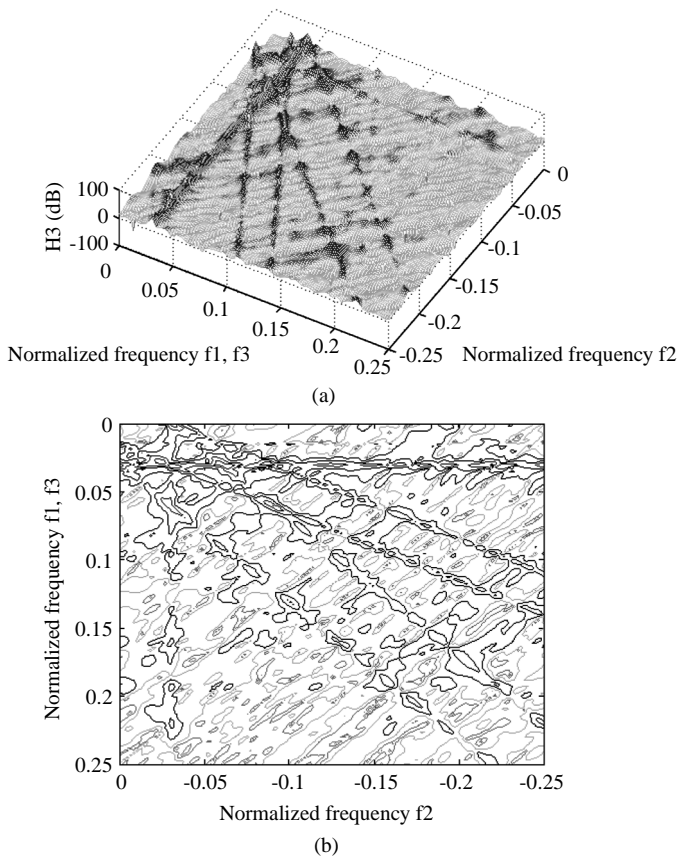


Fig. 14 The third-order GFRFs of thrust-speed model: (a) top view, and (b) contour

frequency is 500 Hz, the actual frequencies are approximately  $f_1 = 16.5$  Hz,  $f_2 = -16.5$  Hz,  $f_1 + f_2 = 16.5$  Hz and  $f_1 + f_2 = -16.5$  Hz. These functions reveal that there appears to be a strong non-linear effect of the system which transfers energy to around 16.5 Hz as defined by the dominant ridges in 16.5 Hz. The results show that all possible frequency combinations are caused by second order non-linear effects (for example cogging torque). This can be confirmed by the power spectral density of the system output in which the power is concentrated on the normalized frequency around 0.033.

The functions  $f_1 + f_2 = 16.5$  Hz and  $f_1 + f_2 = -16.5$  Hz can be seen as a resonance behavior, where energy at the input frequencies  $f_1$  and  $f_2$ , which satisfy  $f_1 + f_2 = 16.5$  Hz,  $f_1 + f_2 = -16.5$  Hz are transferred to  $\pm 16.5$  Hz frequencies. In other words, short time events are transferred to long time events. In contrast, the functions  $f_1 = 16.5$  Hz and  $f_2 = -16.5$  Hz can be seen as a release of energy phenomena, in which input frequency components close to  $\pm 16.5$  Hz are amplified by the system and transferred to frequency components in the output other than  $\pm 16.5$  Hz.

The third-order transfer functions  $H_3(f_1, f_2, f_3)$

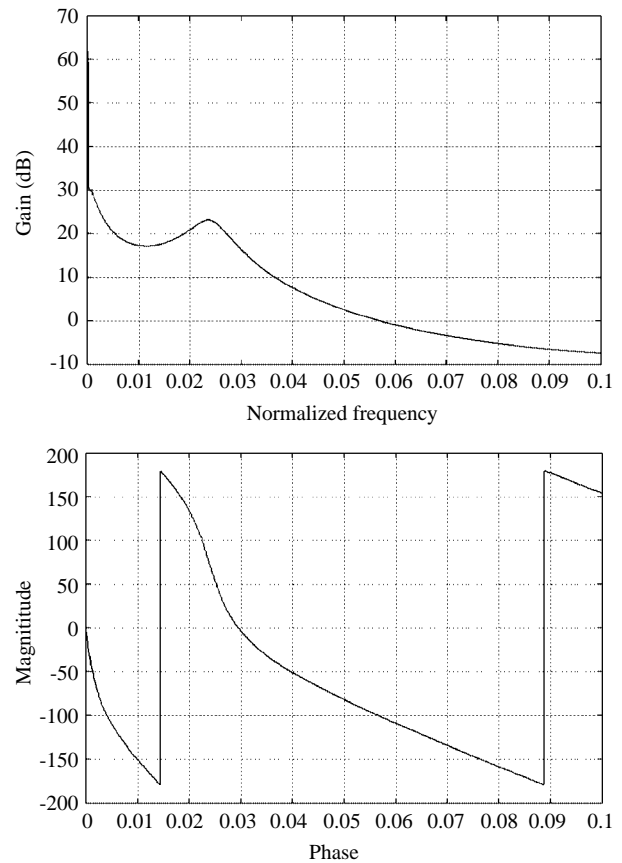


Fig. 15 The first-order GFRFs and phase angle of thrust-position model

illustrated in Fig. 14 for  $f_1 = f_3$  show a similar type of amplification. The low frequencies are amplified, particularly on the ridges of normalized frequency  $f_1 = 0.033$ ,  $f_2 = -0.033$ ,  $f_3 = 0.033$ ,  $f_1 + f_3 = \pm 0.033$  and  $f_1 + f_2 + f_3 = \pm 0.033$ . The true values would be found as defined by  $f_1 = 16.5$  Hz,  $f_2 = -16.5$  Hz,  $f_3 = 16.5$  Hz,  $f_1 + f_3 = \pm 16.5$  Hz and  $f_1 + f_2 + f_3 = \pm 16.5$  Hz. The interpretation of  $H_3(f_1, f_2, f_3)$  is similar to that of  $H_2(f_1, f_2)$  because the frequency ridges listed above correspond to the same type of dynamic effects. The functions  $f_1 = 16.5$  Hz and  $f_2 = -16.5$  Hz can be seen as a release of energy phenomena, and the frequency combinations  $f_1 + f_3 = \pm 16.5$  Hz and  $f_1 + f_2 + f_3 = \pm 16.5$  Hz can be seen as a resonance behavior.

In position NARMAX model, the first-order GFRFs is illustrated in Fig. 15, including two high amplifications at 62.15 dB and 23.13 dB for low normalized frequencies 0 and 0.023 respectively. The sampling frequency of this case is also 500 Hz, multiplied by these normalized frequency lines, and the true values would be found as defined by 0 Hz and 11.5 Hz. The magnitude of the second-order GFRFs  $H_2(f_1, f_2)$  also shows two high magnitudes along the normalized frequencies  $f_1$  and  $f_2$ , defined by  $f_1 = 0$ ,

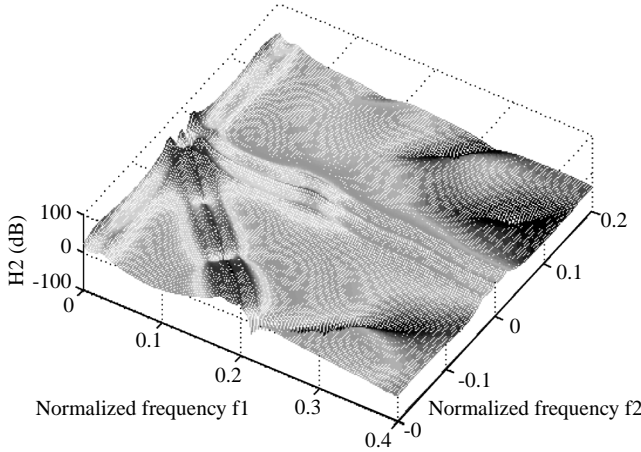


Fig. 16 The second-order GFRFs of thrust-position model

$f_2 = 0, f_1 = 0.023, f_2 = \pm 0.023, f_1 + f_2 = 0$  and  $f_1 + f_2 = \pm 0.023$  (Fig. 16). The true values would be found as defined by  $f_1 = 0$  Hz,  $f_2 = 0$  Hz,  $f_1 = 11.5$  Hz,  $f_2 = \pm 11.5$  Hz,  $f_1 + f_2 = 0$  Hz and  $f_1 + f_2 = \pm 11.5$  Hz.

These functions represent a strong non-linear effect as compression and expansion of energy. The functions  $f_1 + f_2 = 0$  Hz and  $f_1 + f_2 = \pm 11.5$  Hz can be seen as resonance behaviors which represent a phenomenon of energy storage, where energy at the input frequencies  $f_1$  and  $f_2$ , which satisfy  $f_1 + f_2 = 0$  Hz and  $f_1 + f_2 = \pm 11.5$  Hz, is transferred to very low frequencies, close to 0 Hz and 11.5 Hz. The functions  $f_1 = 0$  Hz,  $f_2 = 0$  Hz,  $f_1 = 11.5$  Hz,  $f_2 = \pm 11.5$  Hz, can be seen as a phenomenon of energy release, in which input frequency components close to 0 Hz or 11.5 Hz are amplified by the system and transferred to frequency components in the output other than these two frequencies. The low frequency components in this case correspond to long time events, which are transferred by non-linear effects to higher frequency or shorter time events.

The third-order transfer function  $H_3(f_1, f_2, f_3)$  illustrated in Fig. 17 for  $f_1 = f_3$  shows a similar type of amplification. The low frequencies are amplified, particularly on the ridges of normalized frequencies  $f_1 = 0, f_2 = 0, f_3 = 0, f_1 = 0.023, f_2 = \pm 0.023, f_3 = 0.023, f_1 + f_3 = 0, f_1 + f_3 = \pm 0.023, f_1 + f_2 + f_3 = 0$  and  $f_1 + f_2 + f_3 = \pm 0.023$ . The true values would be found as defined by  $f_1 = 0$  Hz,  $f_2 = 0$  Hz,  $f_3 = 0$  Hz,  $f_1 = 11.5$  Hz,  $f_2 = \pm 11.5$  Hz,  $f_3 = 11.5$  Hz,  $f_1 + f_3 = 0$  Hz,  $f_1 + f_3 = \pm 11.5$  Hz,  $f_1 + f_2 + f_3 = 0$  Hz and  $f_1 + f_2 + f_3 = \pm 11.5$  Hz.

It is important to note that even though the models analyzed are different in terms of model structure, all the models generated give almost identical GFRFs. The frequency ridges are regarded as resonant peaks and they can be verified by the PSD plots. Besides, the frequency domain response functions are seen as invariants of a non-linear system.

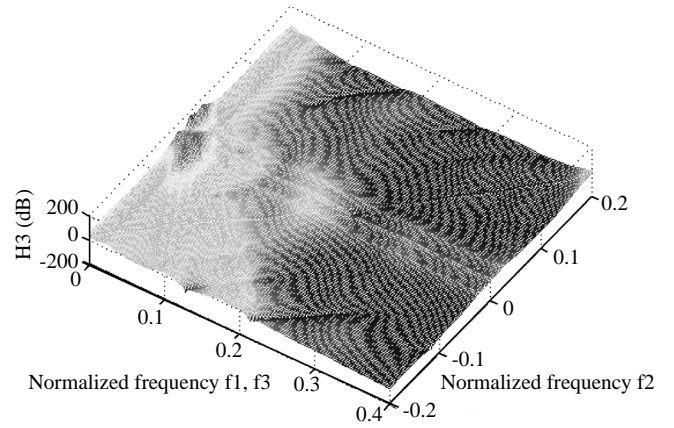


Fig. 17 The third-order GFRFs of thrust-position model

## VI. CONCLUSIONS

A combined time and frequency domain identification approach is considered in this study to analyze data from a PMSM. The NARMAX methodology has been applied to two systems. The first one utilizes the electromagnetic thrust as input and the rotor speed as output, where the second one utilizes the rotor position as output. It has been shown that this motor system, which is non-linear for the considered operating points and electromagnetic thrust, can be modeled with a series of discrete-time NARMAX models, derived for various conditions and constraints.

Applying the NARMAX methodology to this type of system is proved to be a good estimation method, and the novelty of the present results relates to the non-linear frequency domain analysis by the high-order GFRFs which are derived for polynomial NARX models. The GFRFs reveal, for the PMSM application, non-linear couplings which represent energy release and storage between input harmonic components taking place at low frequency and also on particular lines of frequency. Analytical expressions for GFRFs for non-linear systems provide a great deal of insight into the relationship between the time and frequency domain representations of non-linear systems and can be used to study the sensitivity of the frequency domain effects due to the parameter variations in the models.

## NOMENCLATURE

$c$	coefficients of NARMAX model
$d$	system time delay
$f$	frequency
$F$	non-linear function
$g$	coefficients of an auxiliary model
$H$	frequency responding function

$k$	time
$m$	number of input
$r$	number of output
$n$	time lag
$S$	all permutations of frequencies
$w$	terms of an auxiliary model
$u$	system input
$y$	system output
$\varepsilon$	residue
$\alpha$	constant vector term
$\delta$	Kronecker delta
$\tau$	time lag
$\phi$	correlation tests

### Superscripts

<i>asym</i>	asymmetry
$\ell$	degree of non-linearity
<i>sym</i>	symmetry

### Subscripts

<i>MPO</i>	model predicted output
$m$	number of input
$n$	order
$p$	order of input
$q$	order of output
$r$	number of output
$u$	system input
$y$	system output
$\varepsilon$	residue

## REFERENCES

- Babak, N. M., Farid, M. T., and Sargos, F. M., 2004, "Mechanical Sensorless Control of PMSM with Online Estimation of Stator Resistance," *IEEE Transactions on Industry Applications*, Vol. 40, No. 2, pp. 457-471.
- Billings, S. A., Chen, S., and Backhouse, R. J., 1989, "Identification of Linear and Non-Linear Models of a Turbocharged Automotive Diesel Engine," *Mechanical Systems Signal Process*, Vol. 3, No. 2, pp. 123-142.
- Billings, S. A., and Voon, W. S. F., 1986, "Correlation Based Model Validity Tests for Non-Linear Models," *International Journal of Control*, Vol. 44, No. 1, pp. 235-244.
- Bolognani, S., Zigliotto, M., and Zordan, M., 2001, "Extended-Range PMSM Sensorless Speed Drive Based on Stochastic Filtering," *IEEE Transactions on Power Electronics*, Vol. 16, No. 1, pp. 110-117.
- Brown, M., and Harris, C., 1994, *Neuro fuzzy adaptive modelling and control*, Prentice-Hall, London, UK.
- Cheng, K. Y., and Tzou, Y. Y., 2004, "Fuzzy Optimization Techniques Applied to the Design of a Digital PMSM Servo Drive," *IEEE Transactions on Power Electronics*, Vol. 19, No. 4, pp. 1085-1099.
- Driss, Y., Mohammed, A., and Abdallah, S., 2001, "A New Position and Speed Estimation Technique for PMSM with Drift Correction of the Flux Linkage," *Electric Power Components and Systems*, Vol. 29, No. 7, pp. 597-613.
- Hattori, S., Ishida, M., and Hori, T., 2001, "Vibration Suppression Control Method for PMSM Utilizing Repetitive Control with Auto-Tuning Function and Fourier Transform," *IEEE Annual Industrial Electronics Society Conference*, Denver, USA, Vol. 1, pp. 1673-1679.
- Jahns, T. M., and Soong, W. L., 1996, "Pulsating Torque Minimization Techniques for Permanent-Magnet AC Motor Drives-A Review," *IEEE Transactions on Industrial Electronics*, Vol. 43, No. 2, pp. 321-330.
- Kadjoudj, M., Abdessemed, R., Golea, N., and Benbouzid, M. E. H., 2001, "Adaptive Fuzzy Logic Control for High Performance PM Synchronous Drives," *Electric Power Components and Systems*, Vol. 29, No. 9, pp. 789-807.
- Kadjoudj, M., Benbouzid, M. E. H., Abdessemed, R., and Ghennai, C., 2003, "Variable Bands Hysteresis Current Controllers for VSI-Fed PMSM Drive," *Modelling, Measurement and Control A*, Vol. 76, No. 1-2, pp. 39-55.
- Kadjoudj, M., Benbouzid, M. E. H., Ghennai, C., and Diallo, D., 2004, "A Robust Hybrid Current Control for Permanent-Magnet Synchronous Motor Drive," *IEEE Transactions on Energy Conversion*, Vol. 19, No. 1, pp. 109-115.
- Lang, Z. Q., and Billings, S. A., 2000, "Evaluation of Output Frequency Responses of Nonlinear Systems under Multiple Inputs," *IEEE Transactions on Circuits and Systems II: Analog and Digital Signal Processing*, Vol. 47, No. 1, pp. 28-38.
- Leontaris, I. J., and Billings, S. A., 1985, "Input-Output Parametric Models for Non-Linear Systems," *International Journal of Control*, Vol. 41, No. 2, pp. 311-341.
- Liu, J. J., Cheng, S. J., Kung, I. C., Chang, H. C., and Billings, S. A., 2001, "Non-Linear System Identification and Fault Diagnosis Using a New GUI Interpretation Tool," *Mathematics and Computers in Simulation*, Vol. 54, No. 6, pp. 425-449.
- Mobarakeh, B. N., Meibody-Tabar, F., and Sargos, F. M., 2001, "Robustness Study of a Model-Based Technique for Mechanical Sensorless PMSM," *IEEE Annual Power Electronics Specialists Conference*, Vancouver, Canada, Vol. 2, pp. 811-816.
- Morimoto, S., Kawamoto, K., Sanada, M., and Takeda, Y., 2002, "Sensorless Control Strategy for Salient-Pole PMSM Based on Extended EMF

- in Rotating Reference Frame,” *IEEE Transactions on Industry Applications*, Vol. 38, No. 4, pp. 1054-1061.
- Solsona, J., Valla, M. I., and Muravchik, C., 2000, “On Speed and Rotor Position Estimation in Permanent-Magnet AC Drives,” *IEEE Transactions on Industrial Electronics*, Vol. 47, No. 5, pp. 1176-1180.
- Thouverez, F., and Jezequel, L., 1996, “Identification of NARMAX Models on a Modal Base,” *Journal of Sound and Vibration*, Vol. 189, No. 2, pp. 193-213.
- Tsang, K. M., and Billings, S. A., 1994, ‘Two-Dimensional Pattern Analysis and Classification Using a Complex Orthogonal Estimation Algorithm,” *IEE Proceedings: Vision, Image and Signal Processing*, Vol. 141, No. 5, pp. 339-347.
- Yue, X., Vilathgamuwa, D. M., and Tseng, K. J., 2003, “Observer-Based Robust Adaptive Control of PMSM with Initial Rotor Position Uncertainty,” *IEEE Transactions on Industry Applications*, Vol. 39, No. 3, pp. 645-656.
- Manuscript Received: Mar. 11, 2005**  
**Revision Received: Aug. 15, 2005**  
**and Accepted: Sep. 09, 2005**

